Reprinted from

NUCLEAR INSTRUMENTS & METHODS IN PHYSICS RESEARCH
Section A

Nuclear Instruments and Methods in Physics Research A 397 (1997) 323–331

Calculation of field distortion by a large-gained avalanche in a gas counter

T. Sakae*, A. Nohtomi

Department of Nuclear Engineering, Kyushu University, 6-10-1 Hakozaki, Higashi-ku, Fukuoka 812, Japan

Received 13 August 1996; received in revised form 17 January 1997

N·H

ELSEVIER

Nuclear Instruments and Methods in Physics Research A 397 (1997) 323–331

ELSEVIER

NUCLEAR INSTRUMENTS & METHODS IN PHYSICS RESEARCH Section A

Calculation of field distortion by a large-gained avalanche in a gas counter

T. Sakae*, A. Nohtomi

Department of Nuclear Engineering, Kyushu University, 6-10-1 Hakozaki, Higashi-ku, Fukuoka 812, Japan

Received 13 August 1996; received in revised form 17 January 1997

Abstract

Simulation performed by using the continuity equation of electrons and positive ions is applied to examine the three-dimensional formation and the time evolution of an electron avalanche in a cylindrical gas counter. The field made by space charge is calculated exactly and concurrently by the relaxation method in the evolution. The gas multiplication for photon detection is consistently estimated for an Ar-based mixture by not using any adjustable parameter for geometrical dependency. Field distortion at the time of the finish of the evolution is studied systematically. The distortion is concentrated in a small region of angle in case of a large diameter of the anode. The shape of the distortion is calculated for several distributions of the initial charge. The distortion is enhanced by the distribution that occupies small area in the transverse plain in the avalanche. Change of the field distortion depending on the anode diameter and the initial charge distribution is shown quantitatively by these calculations. The transition to a streamer by the continuous supply of electrons is suggested to depend strongly on the charge distribution in an avalanche.

Keywords: Gas counter; Avalanche; Simulation; Continuity equation; Field distortion; Space charge effect

1. Introduction

Distorted field by space charges presents difficulties in finding a formal solution of the equation describing the ionization growth of a large-gained electron avalanche in a gas. Some numerical methods for simulating the growth of an electrical discharge had been reported mainly for plane parallel electrodes [1,2]. In order to explain the growth in a cylindrical gas counter, "self-induced space-charge effect" was investigated by Mori et al. [3]. In this investigation, the distorted field was estimated by analytical formula obtained with the assumption that the space charges were distributed uniformly around the anode with cylindrical symmetry. For the quantitative study of the effects induced by the distorted field in a cylindrical gas counter, it is necessary to apply a method considering three-dimensional electric field in the cylindrical geometry. Even in the recent works using Monte-Carlo method [4,5], the systematic study of the space-charge effect was not achieved enough because of the relatively large load in computing.

Concerning the large-gain region of a gas counter that contains the proportional and limited proportional region, there has been a considerable interest in the mechanism of the transition to the self-quenching streamer (SQS) [6]. To understand the mechanism, it is important to investigate the field distortion for a large-gained avalanche. In the present work, the characteristic curve method with continuity equations is applied to study the large-gained avalanche in a cylindrical gas counter. It is convenient to use this method for the calculation in the field with a steep increase because of the use of flexible mesh structure and relatively small numerical error.

2. Method of calculation

The calculating model for the electron avalanche incorporates electron bombarded ionization, electron drifting, electron diffusion, space-charge effect on the electric field and electron-ion recombination. Photoionization and electron attachment are not considered as independent processes. The ionization coefficient involves the effects of the processes. Ionic drift is not considered because the time range of this calculation is relatively small in comparison with the drift time. The external circuit is assumed to have an infinite capacitance to accept the output current. The randomness of

* Corresponding author.

PII S0168-9002(97)00771-7

the number of the initial charges and of the multiplication factor are not included in this model. For a field with steep spatial change, the calculation of electron avalanches has to include the dynamic change of electron-swarm parameters in the short-time development of the avalanche. Furthermore the strong distortion of the field should make an inequilibrium condition for the electron momentum transfer in the avalanche. It is not easy to estimate the exact change of the parameters in the condition. For simplicity, the general expression of the continuity equation is used with equilibrium transport coefficients which depend on the electric field and gas pressure. In the high-field region, this assumption will cause errors in the quantitative estimate.

2.1. Continuity equation and characteristic curve method

Electrons and single-charged positive ions are considered as elemental particles of the discharge in a gas counter. The continuity equations describing the growth of an avalanche are

$$\frac{\partial n_e}{\partial t} + \operatorname{div} n_e \boldsymbol{W} = \alpha n_e W + D\Delta^2 n_e - \rho_e n_e n_+, \tag{1}$$

$$\frac{\partial n_+}{\partial t} = \alpha n_e W - \rho_e n_e n_+, \tag{2}$$

where n_e and $n_+(\mathrm{cm}^{-3})$ are the electron and positive-ion densities, $W(=|\boldsymbol{W}|)$ (cm/s) is the drift velocity of electron, $\alpha(1/\mathrm{cm})$ is the Townsend first ionization coefficient, $D(\mathrm{cm}^2/\mathrm{s})$ is the electron diffusion constant and $\rho_e(\mathrm{cm}^3/\mathrm{s})$ is the recombination coefficient. Secondary electron generation at the surface of the cathode electrode due to photon incidence is assumed to be negligible. The existence of excited neutral molecules or atoms and negative ions is excluded for simplicity.

The characteristic curve method is adopted to solve the equation numerically [1]. The following equations are derived from Eqs. (1) and (2) by temporary omission of the diffusion and the recombination terms.

$$n_e(\boldsymbol{r}, t + \Delta t) = n_e(\boldsymbol{r} - \boldsymbol{W}\Delta t, t)\exp(A\Delta t),$$
$$A = \alpha W - \operatorname{div} \boldsymbol{W}, \tag{3}$$

$$n_+(\boldsymbol{r}, t + \Delta t) = n_+(\boldsymbol{r}, t) + \alpha W n_e(\boldsymbol{r} - \boldsymbol{W}\Delta t, t)\Delta t. \tag{4}$$

The particle density is calculated by using Eqs. (3) and (4) on the coordinate system moving on the characteristic curve that goes along the drift movement of particles. On a position given by going back to t from $t + \Delta t$, the required values of the particle density are found by the volume-weighted interpolation using values on the crossing of the lattice. The parameters α and W are defined by using the electric field strength $E(\mathrm{V/cm})$ obtained by interpolation with weight of volume in the space lattice.

The divergence of the drift velocity vector is obtained approximately on the assumption that the infinitesimal changes of azimuthal and axial components are small:

$$\operatorname{div} \boldsymbol{W} = \frac{W_r}{r} + \frac{\partial W_r}{\partial r}, \tag{5}$$

where W_r (cm/s) is the radial component of the drift vector.

The change of electron density by diffusion is obtained by using an equation

$$\Delta n_{e,d} = D\left(\frac{1}{r^2}\frac{\partial^2 n_e}{\partial \theta^2} + \frac{\partial^2 n_e}{\partial z^2}\right)\Delta t, \tag{6}$$

where the effect of the radial diffusion is assumed to be negligible as compared with the drift effect. The equation is converted into a differential equation to obtain a numerical solution.

The change of the electron density by recombination is calculated by the equation

$$\Delta n_{e,r} = -\rho_e n_e n_+ \Delta t. \tag{7}$$

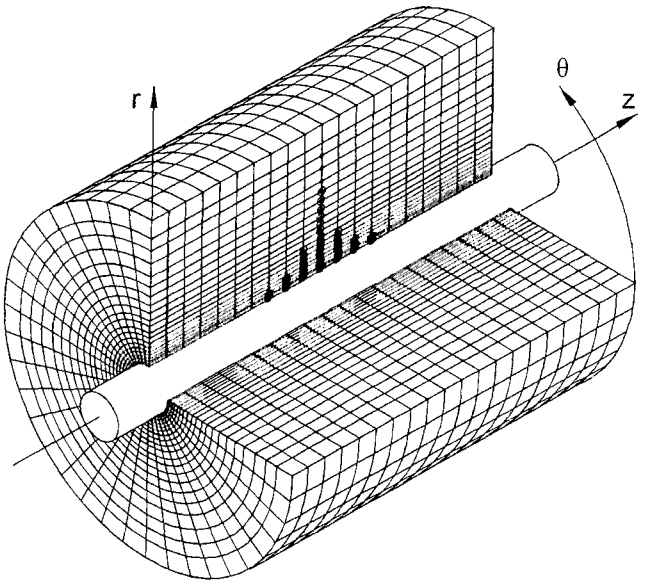

Fig. 1. Space lattice used for representation of an avalanche in a gas counter and geometrical arrangement of electrodes.

The space in a gas counter is divided into mesh as shown in Fig. 1 schematically. The region of the lattice used in the calculation for the particle densities is restricted within the maximum radius ($r_m = 1$ mm) to reduce the load on the computer. In the outside region ($r \geq r_m$), the electric field is not sufficient to generate ionization. The calculating limits along z-axis and the azimuthal circle (1 mm × 360°) are divided into 20 and 40 meshes.

The radial limit is divided into 70 meshes between anode radius and r_m. The outer region extending to the cathode surface is divided into 10 meshes for the field calculation. The intervals of the radial meshes are made to be proportional to radial position r. This means that the intervals have a fixed value on the logarithmic scale of radius. The cathode radius is set to 6 mm for comparison with experimental data.

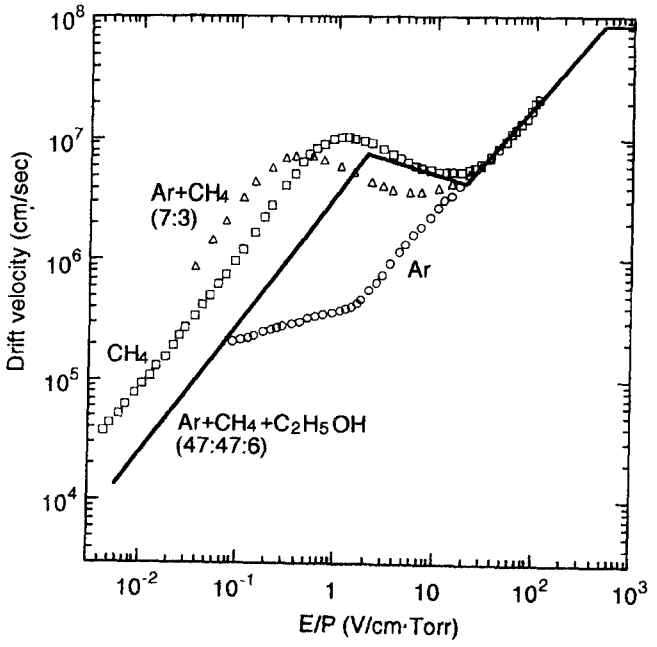

Fig. 2. Electron drift velocity in Ar-based mixtures. Solid line is expected for a gas mixture in this work.

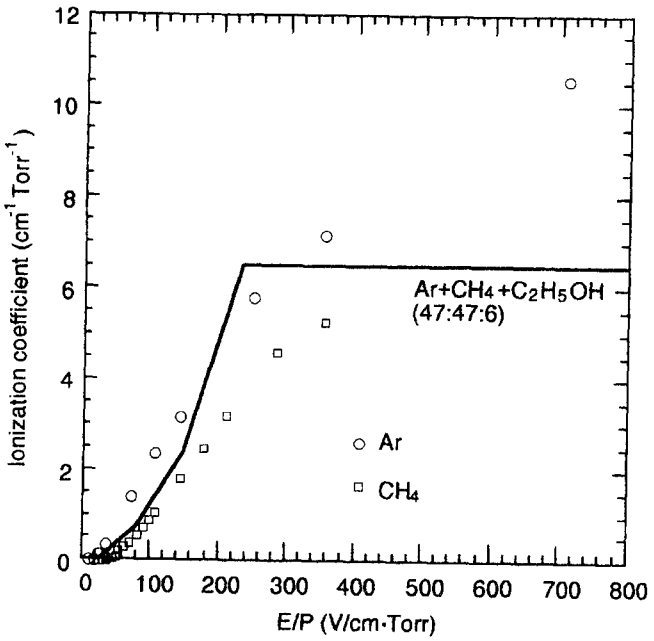

Fig. 3. Ionization coefficient in Ar-based mixtures. Solid line is the estimated value for a gas mixture.

The electric field is obtained by the relaxation method to satisfy Poisson's equation in the three-dimensional lattice structure. In the method, the effect of the induced charge on the surface of electrodes is considered. The field calculation is performed once in several Δt steps of the calculation in order to consider change of the space-charge effect.

2.2. Electron swarm parameter

The swarm parameters are evaluated in this work for an Ar-based gas mixture ($Ar : CH_4 : C_2H_5OH = 47 : 47 : 6$) at atmospheric pressure. The electron drift velocities in the mixture are estimated by using the previous experimental data for Ar-based mixtures [7–9] as shown in Fig. 2, on the basis of comparison with the data measured by Widodo et al. [10] for a similar mixture. The ionization coefficients are synthesized with a set of equations of the first degree which forms a polygonal line. In order to decide the coefficient in the equations, the gas multiplication factor is calculated simply for several cases of the line by using an integration of the ionization coefficient along the evolution of an avalanche. The line is adopted which gives consistent values of the multiplication factor in the proportional region in comparison with the experimental data. The experimental data are given by extrapolation using the data in the large-gain region described in Section 3. The data are corrected by a modification, considering the effect of the pulse shape of the current [11] that flowed out from the anode of the counter. The result of the estimate is shown in Fig. 3 with the previous experimental data for Ar and CH_4 [12,13].

The diffusion coefficient D of electrons is approximately defined as the product of the electron mobility μ and the characteristic energy ε (eV) for an electric field E,

$$D = \varepsilon\mu, \qquad \mu = \frac{W}{E}, \tag{8}$$

where drift velocity of electrons is given by a set of simple functions. The characteristic energy is fixed to 7 eV for the gas mixture in this work because the change in the energy is small in the field region of interest. The recombination factor is established as a constant value of 10^{-7} cm^3/s for simplicity.

2.3. Principal flow of the calculation

The initial charges are arranged around a point located on 0.65 mm apart from the anode in radial direction, 180° azimuthal angle and 0.5 mm axial distance as shown in Fig. 4. The distribution (a) is used as a standard in the present calculations. The dimension of homogeneous density area for the distribution is 0.2 mm (r) × 18° (θ) × 0.2 mm (z). The distribution (b) is just on the point. In the cases of (c)–(e), the distributions have 0.5 mm length in r, θ and z directions, respectively. This length is approximately corresponding to the maximum range of 5.9 keV photo-electron emitted in the gas. These distributions are utilized in the calculation for 50 μm anode diameter in order to study the effects of initial charge distribution on the gas multiplication.

The total number of the initial electron-ion pairs is set to 197. The particle densities are calculated from Eqs. (3)–(5) and (7). After the calculations for all lattice points, the contribution of electron diffusion is obtained by Eq. (6). These calculations are repeated until the total electron charge became small (0.1%) compared to the initial value. The

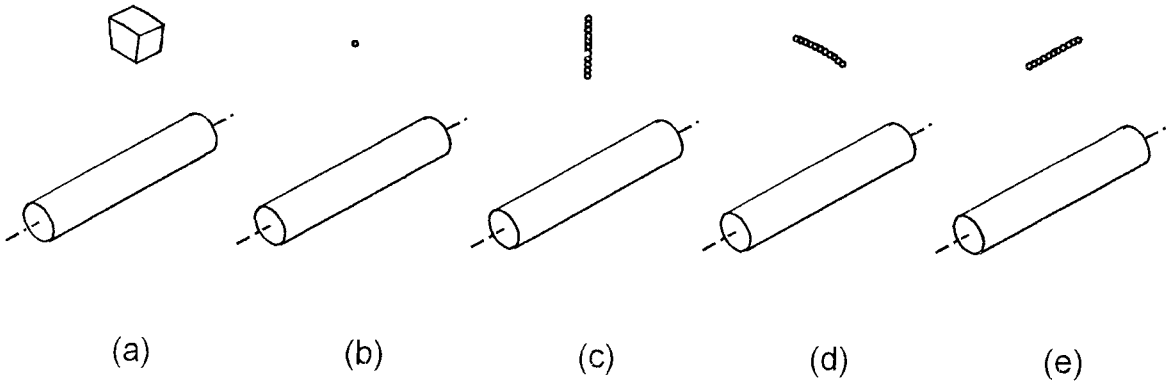

Fig. 4. Initial charge distributions.

number of repetitions was typically 1000 in almost all cases of this work.

Near the anode surface, the time step Δt must be small because of small space mesh and fast electron drift. The space to be calculated is divided into three cylindrical regions with different values of infinitesimal change of time Δt. In the inner region, the value of Δt is smaller than that of the outer region by a factor of integer. The calculations in the outer region are performed after the repetition of those in the inner region in order to get a matching in the time scale. The boundary condition on the surface facing the outer region is kept constant during calculations for the inner region. The inversed-gradient of the electric field frequently makes an instability of the calculation. The instability extends to an overflow of the variable for the number of particle. In order to avoid the instability of the calculation in the region with large field distortion, multiplication is prohibited at the position where the value of field gradient is less than 2.0×10^{7} V/cm^2. In other words, the ionization coefficient is made to zero in the region. By this procedure, the accumulation of charged particles is avoided for an inversed-gradient region of the electric field. The multiplication is also prohibited in the area where the electric field is less than 10% of the initial value of the field. The area where the multiplication is prohibited corresponds to the plasma area in the two-region model studied in previous works [14].

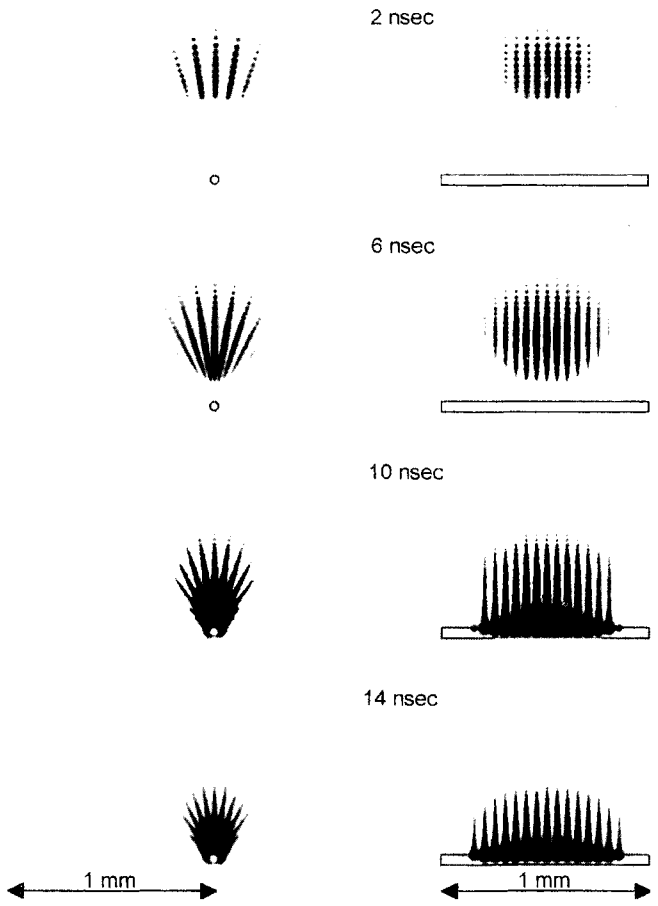

Fig. 5. Time evolution of an avalanche in a cylindrical gas counter.

3. Results and discussion

3.1. Time evolution and gas multiplication

The result of the time evolution of an avalanche is shown in Fig. 5 for 50 μm anode diameter. The anode voltage was set to 2400 V for this calculation. The size of the closed circle shows electron density in the logarithmic scale that becomes zero at 10^{-15} C/cm^2. The maximum charge density that was given at the anode surface was about 10^{-5} C/cm^3 for this anode size. After the quenching of the avalanche, the azimuthal width of ion distribution was about 62° in FWHM for the initial distribution (a). The estimate was achieved by integrating the space charge in the direction of z-axis. The width on z-axis, which was given by integrating the space charge in the azimuthal direction, was 0.35 mm. In most cases of calculations the evolution was terminated on the surface of the anode as shown in Fig. 5. The positive charge density and radial electric field strength on the center axis of

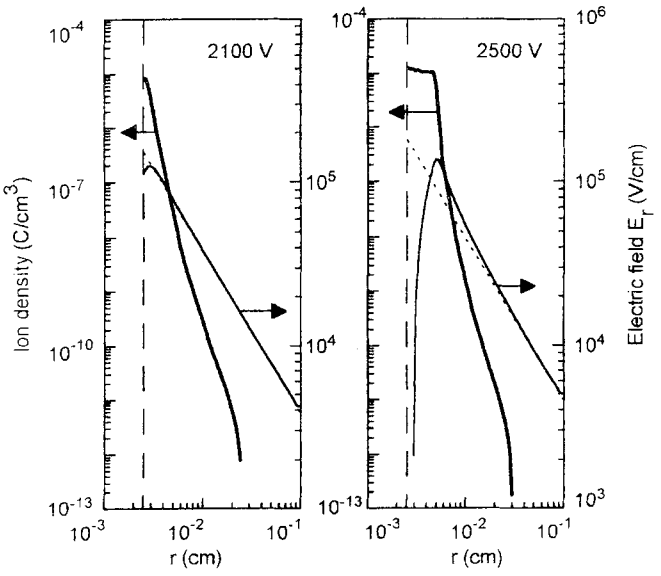

Fig. 6. Positive charge distribution (thick solid line) and electric field strength (normal solid line) on the center line along the avalanche evolution at the end of the multiplication. The field without space charge is drawn by dotted line. The distorted field goes down to negative value at the anode surface for 2500 V anode voltage.

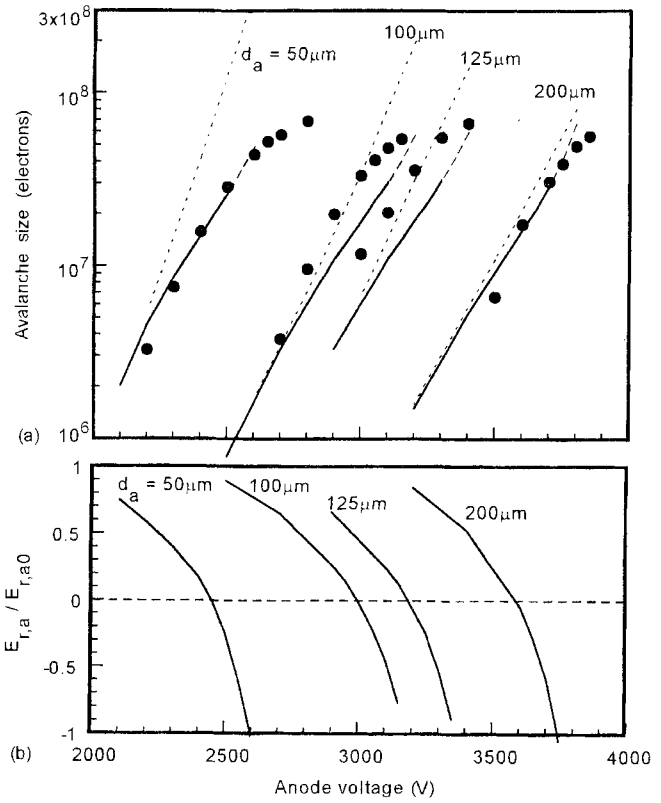

Fig. 7. (a) Avalanche size for an Ar-based gas mixture at large-gain region for ^{55}Fe X-rays detection. The closed circles show experimental data. Solid and dashed lines show the result of the calculation. Dotted line is the result with disregard for the space-charge effect. (b) Normalized radial component of the electric field on the surface of the anode.

the quenched avalanche are displayed in Fig. 6 for 2100 and 2500 V anode voltage. The radial component of the electric field without space charge is drawn by a dotted line. The space-charge effect is creating a low-field region near the surface of the anode. For anode voltage of 2500 V, the field is changed to minus value. The field is not only weakened near the anode surface but also enhanced in the outside region of the charge distribution. The restriction for stability of calculation makes the ion density flat in the high-field region. The saturated value of the ion density is about 10^{-5} C/cm^3. The starting point of ionization can be identified in the figure as a steep rise in ion density at the radius of about 0.3 mm.

The results for avalanche size are shown in Fig. 7(a). The closed circles show experimental results which are corrected for the effect of rising time of current pulse. Dotted line is the result with disregard for the space-charge effect. The space-charge effect in the multiplication can be recognized to have difference for the different anode diameters. That is the saturation effect which is relatively large for a small diameter anode. The change in the avalanche size is about one decade in the saturation region for 50 μm anode diameter. For a large diameter, the change is not as large as the results for the thin anode. In all cases of anode diameter, the slope of increase in the gas gain changes in the higher voltage region as indicated by the dashed line. This increase in gas gain is caused by the partial distortion of field as described in the next section. Overall agreement of the calculation with the experimental data can be achieved for different anode voltages and different anode diameters with no geometrical parameter. The systematic discrepancy between experiments and calculations appeared for 100 and 125 μm anode diameters. This seems to be caused by the real diameter of the anode which is different from the value called in commercial. The saturation of experimental data is under the influence of the fluctuation of the avalanche size caused by statistics of initial charge and multiplication. Because the calculations are not including the effect of fluctuation of the avalanche size, the comparison may not be simple between the calculation and the experiments. After the quenching of the discharge, radial component of the electric field $E_{r,a}$ on the surface of the anode is shown as a function of the anode voltage in Fig. 7(b) for the center of the avalanche. The plotted values of the field strength are normalized to the fields without space-charge effect $E_{r,a0}$. In connection with the streamer transition advocated by Meek [15], the anode voltage V_z giving zero field on the anode surface is useful as an index for checking the characteristics of discharge in the transition region. The field distortion can be compared for different geometries by using this zero field voltage V_z.

3.2. Field distortion

In order to study the field distortion which appears just after the quenching of the discharge, the voltage V_z described

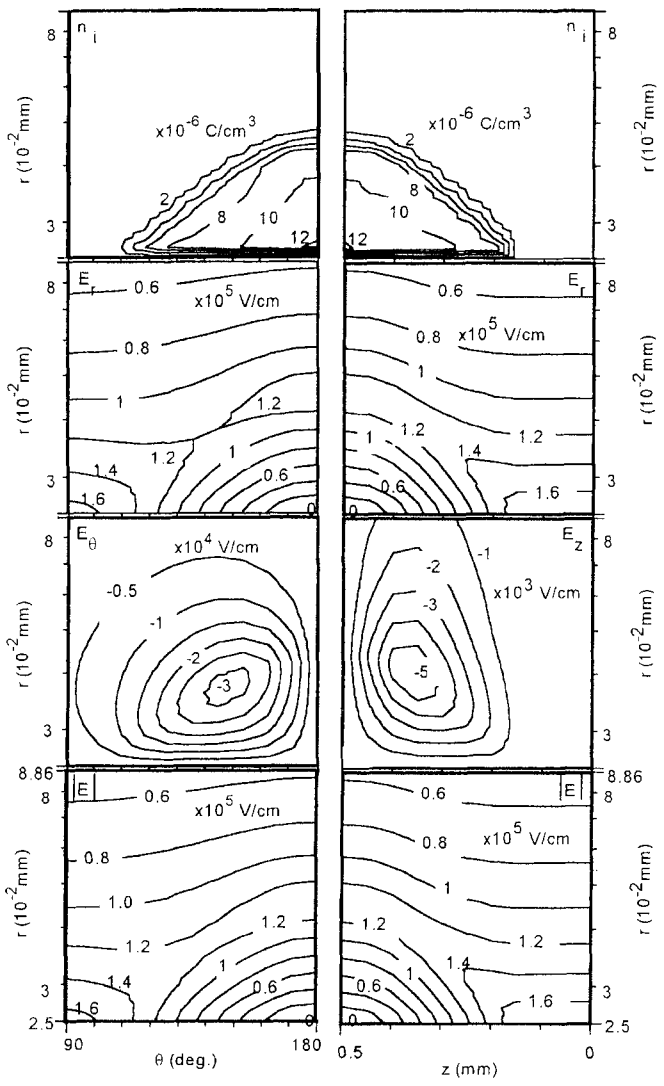

Fig. 8. Contour maps of the ion density, electric field E_r, E_θ, E_z and absolute value of the field for 50 μm anode diameter.

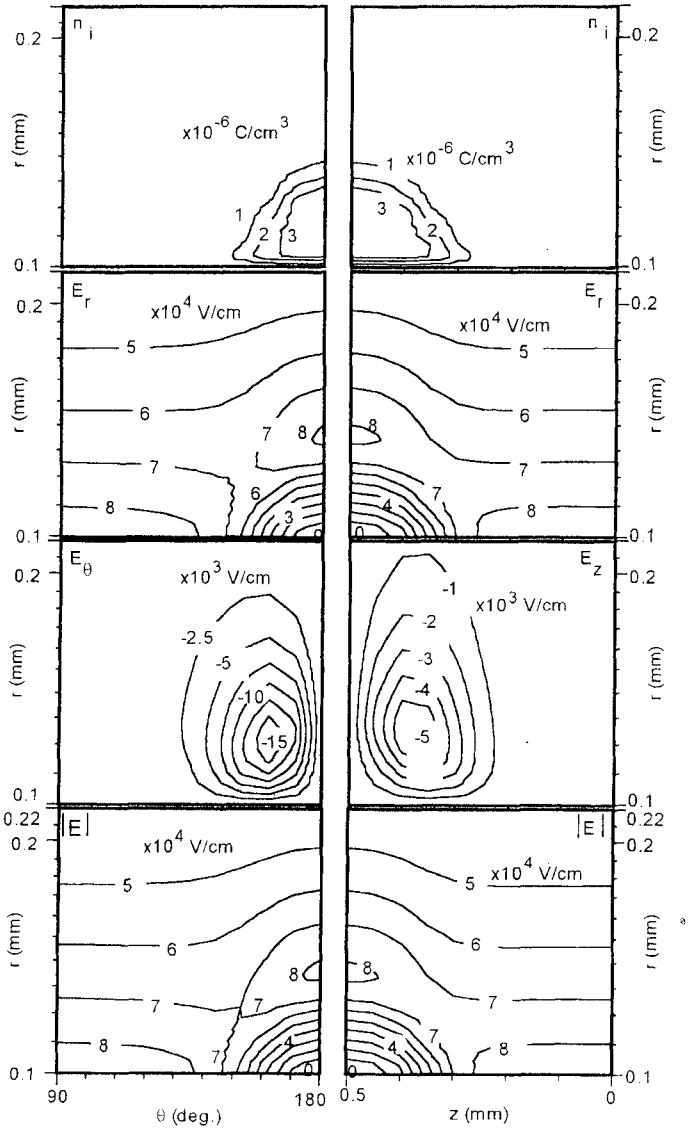

Fig. 9. Contour maps of the ion density, electric field E_r, E_θ, E_z and absolute value of the field for 200 μm anode diameter.

above is set for the respective anode size. Contour maps of ion density, electric field component of the r direction, the component of the θ direction, the component of the z direction and absolute value of the field strength are shown in Fig. 8 for 50 μm anode diameter. The voltage V_z was 2450 V in this case. The two figures have horizontal axes of θ and z, respectively. The vertical axis is the radial distance scaled in logarithm. Here, FWHM is 63° in the θ direction for the distribution which is integrated in the direction of z. The width is 0.35 mm in the z direction for the distribution integrated in the direction of θ. Electric field on the surface of the anode is decreased to zero by the space-charge effect as described in the definition of V_z. The electric field components in the θ and z directions are working for gather the discharge to the center. But, the strength of the fields is much less than the component of the r direction. It is remarkable that the field strength is enhanced over 120% in the outer region of the ion distribution ($r \sim 50$ μm, $\theta = 180°$, $z = 0.5$ mm). The ion density and the field distortion for 200 μm anode diameter are shown in Fig. 9. The voltage V_z is 3590 V. FWHM is 32° in the θ direction and 0.27 mm in the z direction for the distributions described above. In the figure, the field strength for 200 μm anode diameter, the enhancement of the field is localized in the small area. A concentrated distortion in a small angular area is presented for a large diameter anode in a comparison between Figs 8 and 9.

The effect of space charge is displayed in Fig. 10 as the difference between the real field strength and the strength with no space-charge effect. The calculation was achieved for several anode diameters by using the anode voltage V_z in order to make comparison in similar condition of the field. The distortion of the field is dispersed for a small anode diameter in the θ direction. The dispersion width for the 200 μm anode is about one-half of that for the 50 μm anode. The distortion of the electric field is shown in Fig. 11 for several initial charge distributions. The anode voltage was set

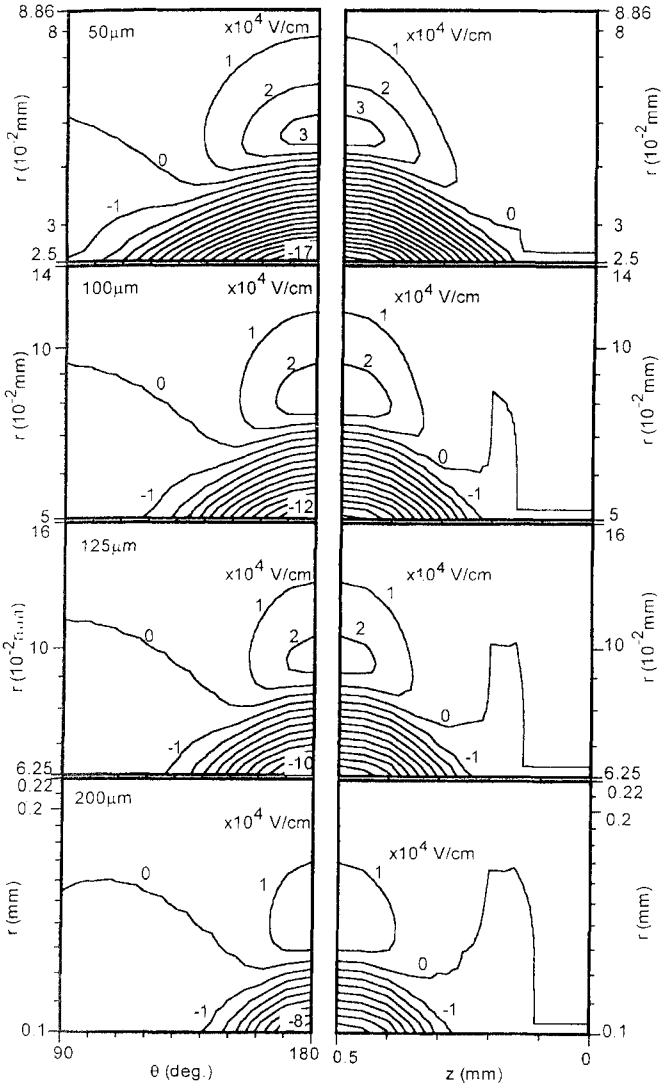

Fig. 10. Contour maps of the difference between the field strength and the initial strength with no space-charge effect for different anode diameter.

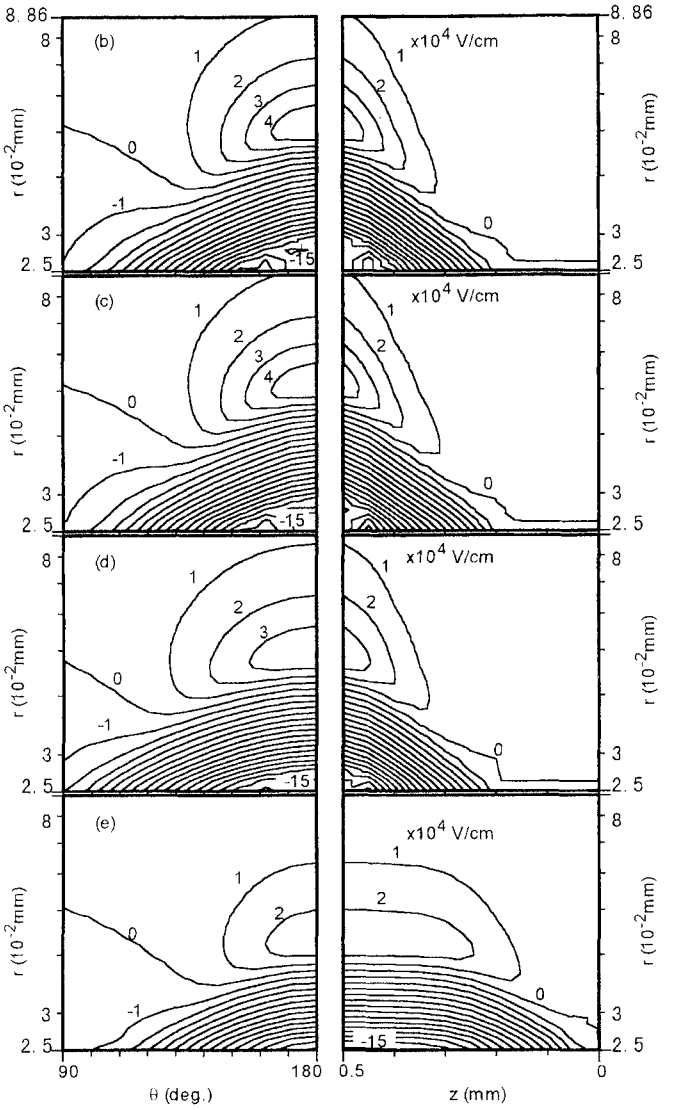

Fig. 11. Contour maps of the difference between the field strength and the initial strength with no space-charge effect for different initial charge distributions.

to 2448 V for these cases with 50 μm anode. The enhancement of the field on the outer region of charge distribution is remarkable for the distribution (b) and (c). It is clarified that the distortion is enhanced by the distribution that occupies a small area in the transverse plain of the avalanche expansion. The enhanced field is about 5×10^4 V/cm for the distribution (b) and (c). It is two times larger than that for distribution (e).

The extension of the dense charge region is shown in Fig. 12 for 6, 8, 10 and 12 ns on which time scale originates the initial charge drifting. The anode diameter was set to 200 μm and the anode voltage was set to 3770 V. By this anode voltage, the avalanche is changing mode described above as a steep increasing of the avalanche size. This is caused by the partial distortion of the field and the supplied electrons flowing into the avalanche as a tail of the space distribution. The shape of the extension looks like that of a streamer. Furthermore, the self-quenching of the extension can be observed in the figure. Because there is no supply of electrons made by photoionization in the calculation, the discharge is expanded very slowly compared with real formation of a streamer (which is terminated in sub-nanosecond).

The avalanche size is saturated by the decreasing field strength near the anode surface, and also increases steeply in higher voltage region by the space-charge effect. The effect was studied in detail for different initial charge distribution. The avalanche sizes are displayed in Fig. 13 as functions of anode voltage for the distributions shown in Fig. 4. For distributions (b) and (c), a large discharge in high-voltage region. This is caused by the partially distorted field at the outer side of the charge distribution. As described above, the real fluctuation of the avalanche size includes the statistical fluctuation in addition to the effect of charge distribution shown in Fig. 13. In the real observation,

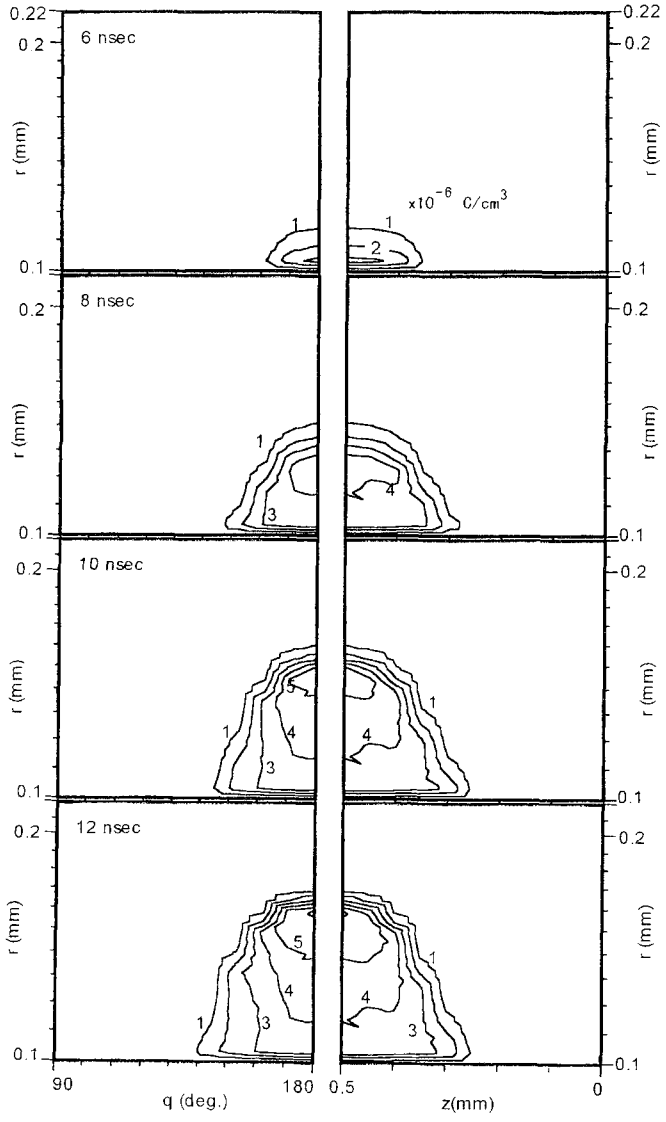

Fig. 12. The extension of the discharge region in the cathode direction.

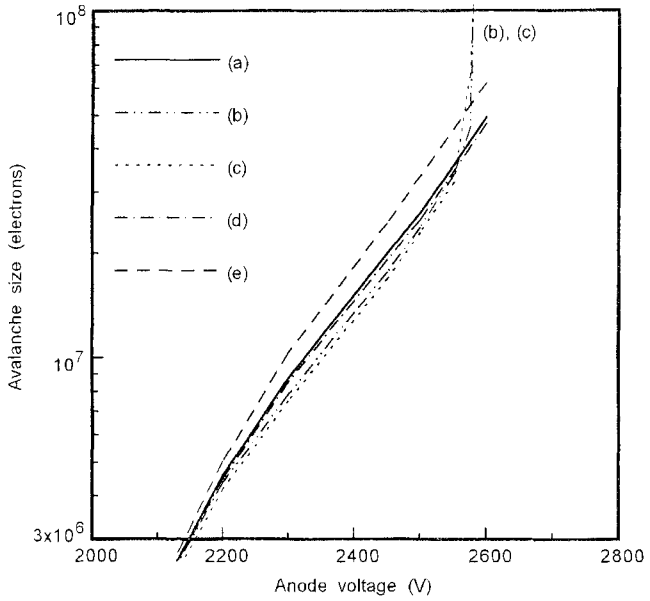

Fig. 13. Avalanche size in an Ar-based gas mixture for different charge distributions. The indices (a)–(e) are the same as those for Fig. 4.

the effect of changing of the initial charge distribution is not seen clearly since the effect of the fluctuation by statistics is dominant. The effect of the initial charge distribution can be seen clearly by this calculation without mixing with others. It is expected that both change of charge distribution and avalanche size are effective on the probability of transition to the large discharge mode. By the rapid supplying of electrons flowing into an avalanche after the increase, this mode should mean the self-quenched streamer.

4. Conclusion

A numerical method has been applied for an examination of large-gained electron avalanche in a gas counter by using equilibrium swarm parameters. As a result of the calculation, the distortion of electric field is estimated in the three-dimensional space of a coaxial cylinder. The simulation is in good agreement with experimental result for gas multiplication factors in the semi-proportional region. The more concentrated distortion in a small area is presented for the larger diameter of the anode. Not only the deviation of the avalanche size but also the arrangement of the initial charge distribution is shown to have a remarkable role in the space-charge effect. This means varieties of the distribution should be considered as one of the conditions for the transition to a streamer in a gas counter. The effect makes different types of contribution for the avalanche formation in two regions of the anode voltage. For lower voltage region, an avalanche with small expansion in θ and z direction loses gain by the field distortion. On the other hand, for higher voltage region, the same charge distribution makes too large a discharge to get a stable solution in the calculation. The field distortion can be grown sufficiently to cause the streamer transition, if electrons are supplied continuously. This means the distortion in an avalanche makes the streamer transition. The condition to reach a streamer transition can be examined without consideration of the electrons supplied after the increase in the discharge.

Acknowledgements

We would like to thank Akira Katase for suggestive discussions. We are also grateful to Ryoji Yamaguchi for his preliminary work of the numerical calculation.

References

[1] A.J. Davies, C.J. Evans, P. Townsend, P.M. Woodison, Proc. IEE 124 (4) (1977) 179.

[2] K. Yoshida, T. Taniguchi, H. Tagashira, J. Phys. D 12 (1979) L3.

[3] C. Mori, M. Uno, T. Watanabe, Nucl. Instr. and Meth. 196 (1982) 49.

[4] J. Groh, E. Schenuit, H. Spitzer, Nucl. Instr. and Meth. A 293 (1990) 537.

[5] P.J.B.M. Rachinhas, T.H.V.T. Dias, F.P. Santos, A.D. Stauffer, C.A.N. Conde, IEEE Trans. Nucl. Sci. NS 41 (1994) 984.

[6] For example, A. Nohtomi, K. Narita, T. Sakae, Y. Uozumi, M. Matoba, N. Koori, IEEE Trans. Nucl. Sci. NS 42 (1995) 552.

[7] Y. Nakamura, M. Kurachi, J. Appl. Phys. 21 (1988) 718.

[8] S.R. Hunter, J.G. Carter, L.G. Christophorou, J. Appl. Phys. 60 (1986) 24.

[9] S.R. Hunter, J.G. Carter, L.G. Christophorou, J. Appl. Phys. 58 (1985) 3001.

[10] S. Widodo, A. Nohtomi, Y. Uozumi, T. Sakae, H. Ijiri, N. Koori, M. Matoba, J. Nucl. Sci. Technol. 29 (1992) 745.

[11] M. Matoba, T. Sakae, Nucl. Instr. and Meth. 219 (1984) 160.

[12] H.N. Kucukarpaci, J. Lucas, J. Phys. D 14 (1981) 2001.

[13] D.K. Davies, L.E. Kline, W.E. Bies, J. Appl. Phys. 65 (1989) 3311.

[14] I. Gallimberti, J. Phys. D 5 (1972) 2179.

[15] J.M. Meek, Phys. Rev. 57 (1940) 722.